29th Congress of the International Council of the Aeronautical Sciences
St. Petersburg, Russia; September 7-12, 2014

OPTIMAL CONTROL SURFACE MIXING OF A RHOMBOID WING UAV

E Miles*, BA Broughton**,
***Council for Scientific and Industrial Research, ****Incomar Aeronautics**
emiles@csir.co.za, bbroughton@incoaero.com

Keywords: *Rhomboid wing configurations, control allocation, control mixing, optimization*

Abstract

This paper presents an overview of the work conducted as part of the design of a control system for a miniature Unmanned Aerial Vehicle (UAV) with a rhomboid wing configuration. The techniques used to design the control allocation and mixing used on the UAV when flying it without artificial stability or control augmentation is provided. The objective of the control mixing was to enable a pilot to operate the UAV as a normal model aircraft during flight testing and as a backup mode should any sensor failures occur later in the flight test program. Although this type of mixing would be straightforward on a conventional airframe, the rhomboid wing configuration has several unique characteristics that complicate the modelling and design process. The resulting mixers also form part of the inner control loops for more sophisticated control modes such as stability augmentation and automatic flight control. The design process made extensive use of mathematical optimization, which is discussed in detail in this paper.

1 Introduction and background

Advanced Technologies and Engineering (ATE) in South Africa, now trading as Paramount Advanced Technologies (PAT), is currently developing a miniature UAV (Unmanned Arial Vehicle) with a rhomboid wing configuration that has already flown in prototype form. The UAV has an expected all-up weight of less than 10 kg in its operational configuration and several propulsion methods and missions are under consideration. The configuration allows for a wide speed envelope and is therefore potentially very flexible in its possible applications.

The configuration used by the UAV has no vertical control surfaces and all control has to be effected via control surfaces on the wings, combined with the throttle. PAT refers to the UAV as the "Roadrunner"; a photograph of the red rhomboid aircraft is shown in Fig. 1. The version shown uses a mini gas turbine as propulsion, but the subject of this paper was powered by an electric motor and conventional pusher propeller.

Fig. 1. PAT Roadrunner UAV

One possible implementation of control on this configuration consists of two control surfaces per flying surface for a total of eight control surfaces, each of which may contribute to roll, pitch and/or yaw control. The distribution of control surfaces on the forward and rear wing also affords the possibility of unconventional control such as direct side-force control, de-coupled pitch and normal force control, or to act as high lift devices. If a total of eight or more control surfaces are utilized as proposed here, redundancy also exists in the control allocation. This redundancy allows for the implementation of degraded control modes so that the UAV can be safely recovered in case of damage or when experiencing certain classes of failures.

There are several approaches to the allocation of control surfaces on this type of UAV. One requirement faced by the design team was that it should be possible to hand-fly the UAV without the use of a feedback control system during flight testing and in a manual backup mode for recovery. This requirement for the rhomboid wing configuration implied the use of control surface mixing in an open-loop control mode where the response to control inputs had to be as conventional as possible. Conventional control through roll, pitch and yaw commands with configuration changes, such as a high-lift configuration for approach and landing, were therefore desired. As this manual flight mode would become the primary backup mode, preferably without any form of active augmentation or feedback, it was decided that some degradation in the flying qualities might be accepted if unavoidable.

The use of optimisation in control allocation has become relatively common, but the particular goals set forth in this work, namely efficient control allocation without the use of feedback loops, and in particular as applied on a rhomboid or joined wing configuration, have received less attention in the published literature. Some examples of recent work related to the use of optimisation in control allocation are briefly listed here. Reference [1] describes the development of a control allocation system which would be used as part of a fault-tolerant control (FTC) system on UAVs. The vital role of that system in diminishing the likelihood of a fault that might originate at the reconfiguration of the control, guidance or navigation systems of the aircraft by minimizing the difference between the desired and achievable aircraft performance parameters is emphasized. This is accomplished through optimization of the control allocation commanded by the virtual actuators to the physical actuators present on the aircraft. Reference [2] implemented a closed-loop system in order to minimize the adverse effects of the trim velocity variation on the stability and performance of a very flexible aircraft. The control design process is expressed as a convex optimization problem by using linear matrix inequality techniques. Reference [3] considered actuator failures due to abnormal changes in the plant or incorrect knowledge of the plant's mathematical structure when certain conditions were violated. Model errors, actuator failures and simultaneous estimation of the plant model were compensated for through a direct adaptation of state feedback gains for state tracking.

In addition to the goals already stated, the project further investigated the use of several levels of control allocation depending on the state information available to the controller and the level of control feedback desired. This approach may be particularly valuable during test flying and when evaluating novel control methods, since it would allow progressive introduction of feedback control loops during flight testing. It will also allow the UAV to revert to a simple fixed gain; open-loop control system for manual flying should any failures occur or unpredictable behaviour is observed. It is further expected that a well-designed open-loop mixing matrix that decouples the primary responses of the UAV will simplify design of the feedback control system. Although control mixing might be relatively simple for conventional configurations, the lack of a vertical control surface, certain inherent characteristics of rhomboid wing configurations and the need to test unconventional control modes, made the control allocation process considerably more challenging. This paper will focus on the open loop problem with no state information available which, therefore, implies a fixed or static control allocation scheme.

Besides providing relatively conventional response to control inputs (except when evaluating specific unconventional control modes) and good flying qualities, it was still desired that all practical constraints be observed in the design of the control allocation and mixer. In particular, control surface saturation had to be avoided and control responses also had to be kept as linear as far as possible.

2 Aircraft modelling

The control allocation design process was highly dependent on an accurate, nonlinear, six degree-of-freedom (6 DOF) model of the aircraft. The creation of an accurate simulation

model for an unconventional configuration such as the one under consideration is a complex task. Several parallel tasks were undertaken to create a custom six-degree of freedom model capable of trimming for various steady-state flight conditions, simulation, linearization, modal analysis and several additional functions. This model was populated with wind tunnel data augmented by analytical predictions and mass and inertia measurements of the actual test airframe. A separate propulsion model was also developed to predict the forces and moments generated by the electric motor/propeller combination. Torque and gyroscopic effects are taken into account, which results in asymmetric responses even for a symmetrical airframe.

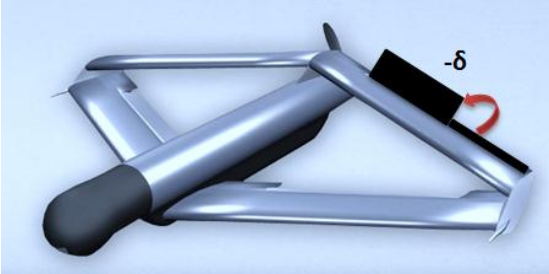

Fig. 2. Roadrunner actuator convention

2.1 Wind tunnel test results

The static aerodynamic coefficients were obtained through wind tunnel testing. The airframe characterization tests were performed using the Modern Design of Experiments (MDOE) technique [5]. MDOE is aimed at extracting as much information as possible from a limited number of tests [6]. In order to limit the amount of wind tunnel testing necessary, a test matrix was designed to capture the response of the airframe utilising a response surface approach. Characteristic response surfaces were derived in the form of mathematical models that were statistically defensible [7]. In order to determine the response surfaces characterising the airframe, the MDOE technique was used as a function of 10 factors, i.e. angle of attack, angle of sideslip, and the deflections of the eight individual control surfaces. The commercially available package Design Expert from Stat-Ease was used to analyse the test data [8]. The static stability was experimentally determined from wind tunnel data using the DOE approach [9]. The MDOE models for the various aerodynamic forces and moments were obtained in the form of coefficients of polynomial expressions. The design space was divided into three angle of attack ranges, which resulted in separate MDOE models valid over each individual range. The low alpha region spanned $-6° \leq \alpha \leq 6°$, the high alpha region spanned $4° \leq \alpha \leq 11°$ and the post stall region spanned $14° \leq \alpha \leq 18°$. The design test envelope for the angle of attack range therefore covered the range $-6° \leq \alpha \leq 18°$ so that the combined MDOE model was defined over the same range. The sideslip design test envelope consisted of a range of $-10° \leq \beta \leq 10°$. The low alpha and high alpha range MDOE models were expressed as 2^{nd} order polynomials with pure 3^{rd} order terms, whereas the post stall region was reduced to a linear model with two additional squared terms. Several asymmetric terms were observed in the MDOE models, which although statistically significant, were undesirable for the flight dynamics modelling of the physically symmetrical airframe. The MDOE models were therefore modified for implementation in the simulation environment by eliminating the asymmetries that resulted from the experimental testing and MDOE analysis technique. In addition, the low, medium and high angle of attack aerodynamic models were combined into a single model using blending functions over the overlapping angles of attack (between the low and high angle of attack sections) and to span the range from 11 to 14 degrees angle of attack, which was not covered by the MDOE models at all. The final model gives each of the six body-axis static aerodynamic coefficients as a function of angle of attack, angle of sideslip and a combination of deflections of the eight control surfaces.

2.2 Stability derivatives

The stability derivatives that were not obtained through the wind tunnel tests were calculated using Athena Vortex Lattice (AVL) [4]. AVL is a software package developed at MIT that is suitable for the aerodynamic and flight-dynamic analysis of rigid aircraft in inviscid, incompressible flow. In order to verify the AVL model, static coefficients predicted by the

AVL model were compared to the wind tunnel results in the low angle of attack range. Despite the expected differences related to the use of a vortex lattice program, correspondence between the AVL and the wind tunnel results were considered of sufficient accuracy to justify the use of the damping derivatives (that could not be obtained in the wind tunnel) in the simulation. Due to difficulties in capturing the side-force and yawing moment coefficient contributions of the fuselage accurately in AVL, additional empirical calculations were used to further augment the dynamic derivatives.

2.3 Flight dynamic modelling

A custom 6 DOF flight dynamics model was implemented in Matlab. The 6 DOF simulations consisted of a complete nonlinear aerodynamic model, an electric motor/propeller propulsion model and a 1976 standard atmospheric model. The static coefficients for the aerodynamic model were obtained from wind tunnel testing, and the dynamic coefficients from vortex lattice analysis and empirical calculations, as already described. The propulsion force and propeller torque were calculated using a custom model appropriate to the brushless motor and measured propeller coefficient tables. Gyroscopic effects were also modelled.

The 6 DOF simulations were used for basic trim calculations, as part of the objective and constraint functions of the optimiser, and as a means for evaluating the resulting control allocation schemes.

In the material that follows, the nominal flight condition used in the optimisation process was for a 30 m/s airspeed and standard sea-level conditions. However, the resulting allocation schemes were tested at off-design conditions that included flight speeds down to the 1g level stall condition.

3 Optimization

The complex and often conflicting mixing requirements necessitated the use of constrained mathematical optimization throughout the design process. The optimization techniques used, as well as the studies used to evaluate the impact of uncertainties in the modelling, is discussed below. The ultimate goal of the project was to optimize the control surface scheduling through the design of a mixing or control allocation function. A custom sequential quadratic programming (SQP) optimization algorithm was used due to its efficiency as a general optimiser for constrained optimisation problems. An alternative leap-frog type of optimization algorithm was also used in selected cases. In general, the SQP algorithm was preferred due to its speed and efficiency, while the leap-frog method was used as a slower but slightly more robust alternative.

3.1 Mixing function

The mixing or allocation function determined the physical deflections of the individual control surfaces as a function of the conventional input commands (roll, pitch and yaw inputs). The general layout of the airframe is illustrated in Figure 3. Note that the control surfaces numbering as shown in the figure will be used throughout the paper.

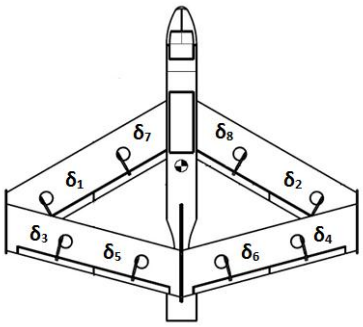

Fig. 3. Roadrunner actuator setup

In order to allow for the possibility of differential control (more up than down movement of a surface), a quadratic mixing function was used. The following equation (in matrix form) was used:

$$\{\delta\} = [\boldsymbol{A}]\begin{Bmatrix}\delta_e{}^2\\ \delta_a{}^2\\ \delta_r{}^2\end{Bmatrix} + [\boldsymbol{B}]\begin{Bmatrix}\delta_e\\ \delta_a\\ \delta_r\end{Bmatrix} + \{T\} \quad (1)$$

In Equation 1, matrices A and B were were used as the quadratic and linear coefficients, respecticaly, while the column vector T was used is a constant trim bias vector $\{\delta_e, \delta_a, \delta_r\}'$ represents the input commands, and for

convenience covered the range -1 to 1. For example, a roll input $\delta_a = -1$ represented a full left roll command while $\delta_a = 1$ represented a full right roll command. The output vector (left-hand side of the equation) represented the eight individual control surface deflections in degrees. The A and B matrices therefore had dimensions 8x3.

3.2 Optimization process

The optimization process consisted of two independent phases. The goal of the first phase was to trim the aircraft, therefore solving for the T vector in Equation 1. The results were then passed to phase 2 and used as a trim bias vector. The goal of the second phase was to determine the individual coefficients in the A and B matrices in Equation 1.

3.2.1 Phase 1

The first phase determined the fixed trim bias vector. Furthermore, the design variables for this phase also included the throttle position ($\delta_{throttle}$), angle of attack (α) and side-slip angle (β). The objective function was defined as the sum of the squares of the control surfaces as shown in equation 2:

$$\boldsymbol{f} = \sum_{\boldsymbol{i=1}}^{\boldsymbol{8}} [\delta_i{}^2] \qquad (2)$$

This objective function implies the minimum combined control deflection to achieve a steady trimmed state. In order to trim the aircraft, the time derivatives of the relative airspeed ($\dot{V}, \dot{\alpha}, \dot{\beta}$) and the three body rotational accelerations ($\dot{p}, \dot{q}, \dot{r}$) were required to be zero. The problem therefore consisted of six equality constraints, i.e. roll acceleration ($\dot{p}$), yaw acceleration ($\dot{r}$), pitch acceleration ($\dot{q}$), angle of attack acceleration ($\dot{\alpha}$), side slip angle acceleration ($\dot{\beta}$) and acceleration of relative airspeed (TAS) ($\dot{V}_t$), all required to be zero:

$$\boldsymbol{h} = \dot{p} = \dot{r} = \dot{q} = \dot{\alpha} = \dot{\beta} = \dot{V}_t = 0 \qquad (3)$$

The trim control surface deflection positions that were obtained were stored in the trim bias vector and used as a constant term throughout the design. The trim bias vector was therefore:

$$\{T\} = \{x_{trim}(i)\}, i = 1{:}8 \qquad (4)$$

No inequality constraints were required and the problem was easily solved using the custom SQP solver.

3.2.2 Phase 2

Phase 2 consisted of various optimizations design trials. The weighted sum method [10] was typically used in the objective function. The objective function was therefore a scalarized multi-objective optimization problem, due to the fact that multiple objectives were placed in one objective function where they were related by weightings. The goal of the optimization problem in phase 2 was to find the optimal mixing coefficient matrices for various design cases.

3.3 Design variables

The optimization problem comprised of 24 design variables. For the symmetrical aircraft, the opposing control surfaces could use the same design variables, while only changing the coefficient signs where appropriate. The mixing matrices containing the design variables were therefore assembled as follows.
Matrix A is defined in Equation 5:

$$\boldsymbol{A} = \begin{bmatrix} x(1) & x(2) & x(3) \\ x(1) & x(2) & x(3) \\ x(4) & x(5) & x(6) \\ x(4) & x(5) & x(6) \\ x(7) & x(8) & x(9) \\ x(7) & x(8) & x(9) \\ x(10) & x(11) & x(12) \\ x(10) & x(11) & x(12) \end{bmatrix} \qquad (5)$$

And matrix B is defined in Equation 6:

$$\boldsymbol{B} = \begin{bmatrix} x(13) & x(14) & x(15) \\ x(13) & -x(14) & -x(15) \\ x(16) & x(17) & x(18) \\ x(16) & -x(17) & -x(18) \\ x(19) & x(20) & x(21) \\ x(19) & -x(20) & -x(21) \\ x(22) & x(23) & x(24) \\ x(22) & -x(23) & -x(24) \end{bmatrix} \qquad (6)$$

The first column in the two matrices represent the coefficients contributing to pitch control, column two to roll control and the third column to directional control.

3.4 Objective function

The objective function for the various cases is defined in equation 7. Both the SQP and leap-frog optimization methods expected minimisation functions, so a negative sign was used where a term had to be maximized.

$$f = -(2w_1\dot{p} + 2w_2\dot{\beta} + w_3\dot{q}_1 - w_4\dot{q}_2) \quad (7)$$

In Equation 7, $\dot{p}$ was the roll rate corresponding to a maximum roll control input, β represented the steady-state sideslip generate by a yaw control input, $\dot{q}_1$ is the pitch response for a maximum positive elevator input (nose up), and $\dot{q}_2$ for a maximum negative elevator input (nose down). The factor 2 for the roll and yaw cases were used to sum the effects of positive and negative inputs, which resulted in similar responses due to the symmetry of the problem.

3.5 Constraints

Various constraints were considered. The most successful combination is presented here.

3.5.1 Equality constraints

The equality constraints consisted of two parts. The purpose of the first part was used to decouple the pitch and side-slip response to a roll command, which considerably improves the handling qualities of the resulting aircraft:

$$h(1) = q \quad (8)$$

$$h(2) = \beta \quad (9)$$

The purpose of the second part was to minimise the pitch and roll response due to a yaw command:

$$h(3) = q \quad (10)$$

$$h(4) = p \quad (11)$$

3.5.2 Inequality constraints

The control surfaces are servo driven, but typical control deflections that can be achieved for this type of aircraft were $-30° \leq \delta \leq 30°$.

Before the control surface constraints could be defined, a close examination of all the control input combinations was done. Preventing saturation for all possible input commands would over-constrain the problem, and a more practical approach was therefore followed. Table 2 was used to evaluate all the possible control input combinations and their practical applicability.

Table 1: Input command combinations

δ_e	δ_a	δ_r	Reqd?	Comment
-1	0	-1	×	Not a realistic input
-1	0	0	✓	Full down elevator
-1	0	1	-	Unlikely combination
-1	1	-1	×	Not a realistic input
-1	1	0	-	Unlikely combination
-1	1	1	×	Not a realistic input
-1	-1	-1	×	Not a realistic input
-1	-1	0	-	Unlikely combination
-1	-1	1	×	Not a realistic input
0	0	-1	✓	Left yaw command
0	0	0	✓	Neutral control
0	0	1	✓	Right yaw command
0	1	-1	✓	Roll + yaw
0	1	0	✓	Right roll command
0	1	1	✓	Roll + yaw
0	-1	-1	✓	Roll + yaw
0	-1	0	✓	Left roll command
0	-1	1	✓	Steady-heading sideslip
1	0	-1	✓	Pos. pitch + yaw
1	0	0	✓	Full positive pitch
1	0	1	✓	Pos. pitch + yaw
1	1	-1	×	Not a realistic input
1	1	0	✓	Pitch + roll
1	1	1	×	Not a realistic input
1	-1	-1	×	Not a realistic input
1	-1	0	✓	Pitch + roll
1	-1	1	×	Not a realistic input

The table was used to determine the command combinations that may result in control surface saturation.

Fourteen realistic combinations were identified and are highlighted in the table above, which

means that each control surface will have 14 constraints. Further inspection revealed that some duplicate terms existed for the corresponding control surfaces on the opposite side of the aircraft. It was possible to further reduce the number of inequality constraints by averaging the contribution of the left and right trim terms. These were slightly different since the control surfaces had to counter propeller torque in the steady trimmed condition, but their magnitudes were close enough to justify the use of averaged values.

$$T_{12} = \frac{1}{2}(T_1 + T_2) \tag{12}$$

$$T_{34} = \frac{1}{2}(T_3 + T_4)$$

$$T_{56} = \frac{1}{2}(T_5 + T_6)$$

$$T_{78} = \frac{1}{2}(T_7 + T_8)$$

Thus only 14 x 4 inequality constraints were required; the inequality constraints for control surface 1 and 2 are defined in the equation below:

$$\begin{aligned}
g(1) &= (x(3) - x(15) + T_{12})^2 - k^2 \\
g(2) &= (x(3) + x(15) + T_{12})^2 - k^2 \\
g(3) &= (x(2) + x(3) + x(14) - x(15) + T_{12})^2 - k^2 \\
g(4) &= (x(2) + x(3) + x(14) + x(15) + T_{12})^2 - k^2 \\
g(5) &= (x(2) + x(14) + T_{12})^2 - k^2 \\
g(6) &= (x(2) - x(14) + T_{12})^2 - k^2 \\
g(7) &= (x(2) + x(3) - x(14) - x(15) + T_{12})^2 - k^2 \\
g(8) &= (x(2) + x(3) - x(14) + x(15) + T_{12})^2 - k^2 \\
g(9) &= (x(1) + x(3) + x(13) - x(15) + T_{12})^2 - k^2 \\
g(10) &= (x(1) + x(3) + x(13) + x(15) + T_{12})^2 - k^2 \\
g(11) &= (x(1) + x(13) + T_{12})^2 - k^2 \\
g(12) &= (x(1) - x(13) + T_{12})^2 - k^2 \\
g(13) &= (x(1) + x(2) + x(13) + x(14) + T_{12})^2 - k^2 \\
g(14) &= (x(1) + x(2) + x(13) - x(14) + T_{12})^2 - k^2
\end{aligned} \tag{13}$$

The approximate indication of maximum deflection that a control surface will experience during a typical flight is given by the *k* terms in the equations, which were typically set to 30 deg.

4 Results

A large number of cases that consisted of various combinations of constraints and weights in the objective function were evaluated. The results presented here are typical for a solution that meets all the design requirements.

4.1 Objective function

The objective function weights were varied in order to determine the optimum aircraft response. The final weights used for the objective function are specified in Table 3.

Table 2: Objective function weights

w_1	w_2	w_3	w_4
0.8	1000	5	0.01

Note that a very large weight was required for the side-slip term. Aerodynamically, the control surfaces were relatively inefficient in generating sideslip, and the optimiser therefore preferred to improve roll-rate, which could easily be achieved with opposing control surface deflections. The importance of nose-down pitch response was reduced by using a small weight for the fourth term. Even with that small term, nose-down pitch requirements are easily achieved. The roll-rate response complies with the handling quality specifications given in reference [11], which was used as a guideline for the desired response. The suitability of the pitch response was evaluated by testing that sufficient control margin still remains for elevator control at the stall condition.

4.2 Constraints

The inequality and equality constraints were all satisfied at the optimum design point. None of the constraints were violated, but a few inequality constraints were active at the optimum point. This is expected as the

optimiser attempts to fully utilise the control power available.

4.3 Mixing function

The mixing function containing the optimum values for the example stated is presented in the equation below.

$$\begin{Bmatrix}\delta_1\\ \delta_2\\ \delta_3\\ \delta_4\\ \delta_5\\ \delta_6\\ \delta_7\\ \delta_8\end{Bmatrix} \tag{14}$$

$$= \begin{bmatrix} 6.8185 & 0.8722 & -1.7409 \\ 6.8185 & 0.8722 & -1.7409 \\ -0.0523 & 5.3675 & -2.4888 \\ -0.0523 & 5.3675 & -2.4888 \\ -4.4326 & -0.2478 & -0.2463 \\ -4.4326 & -0.2478 & -0.2463 \\ 2.9761 & 0.5315 & -1.6061 \\ 2.9761 & 0.5315 & -1.6061 \end{bmatrix} \begin{Bmatrix} {\delta_e}^2 \\ {\delta_a}^2 \\ {\delta_r}^2 \end{Bmatrix}$$

$$+ \begin{bmatrix} 7.7205 & 13.7203 & -16.2820 \\ 7.7205 & -13.7203 & 16.2820 \\ -13.3924 & 18.8118 & 10.9529 \\ -13.3924 & -18.8118 & -10.9529 \\ -21.0555 & 0.0009 & -0.0002 \\ -21.0555 & -0.0009 & 0.0002 \\ 10.2066 & 12.6510 & -14.7875 \\ 10.2066 & -12.6510 & 14.7875 \end{bmatrix} \begin{Bmatrix} \delta_e \\ \delta_a \\ \delta_r \end{Bmatrix}$$

$$+ \begin{Bmatrix} 0.7409 \\ 0.9969 \\ -3.4924 \\ -2.7357 \\ -4.421 \\ -4.1108 \\ 3.559 \\ 3.7139 \end{Bmatrix}$$

The aircraft's handing was evaluated by implementing this mixing function in the simulation. The results are discussed in the following section.

4.4 Six DOF simulation

The results for the various evaluations utilising the optimiser results are described here.

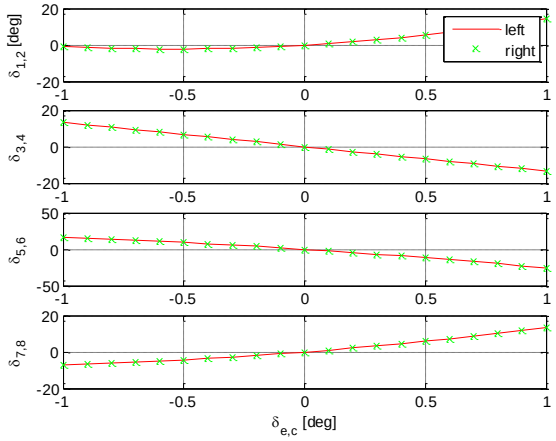

Fig. 4. Elevator mixing

Figure 4 presents the control surface positions resulting from a range of elevator-only inputs. It can be seen that the two inner control surfaces (δ_5 and δ_6) on the rear wing are primarily responsible for the aircraft's pitching moment. Most of the pitch control is effected by the inner control surfaces. The outer control surfaces on the front (δ_1 and δ_2) and rear wings (δ_3 and δ_4) are barely utilized for pitch control. Although the outer control surfaces can also contribute to the total pitching moment, the optimiser tended to reserve their use for roll and yaw control.

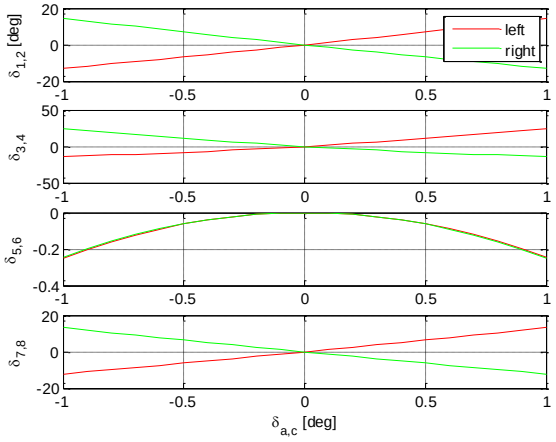

Fig. 5. Aileron mixing

Figure 5 presents the control surface positions for a range of aileron-only inputs. It can be seen that all the control surfaces on the left front and left rear wing are deflected downwards (positive deflection as defined earlier), and all the control surfaces on the right front and right rear wing are deflected upwards generating a positive roll

input resulting in the aircraft banking to the right. The differential control can be seen on close inspection, by evaluating the amount to which the corresponding control surfaces on the left and right deflect. The figure also shows that control surfaces 5 and 6 are barely used for rolling the aircraft, as these were mostly reserved by the optimiser to effect pitch control.

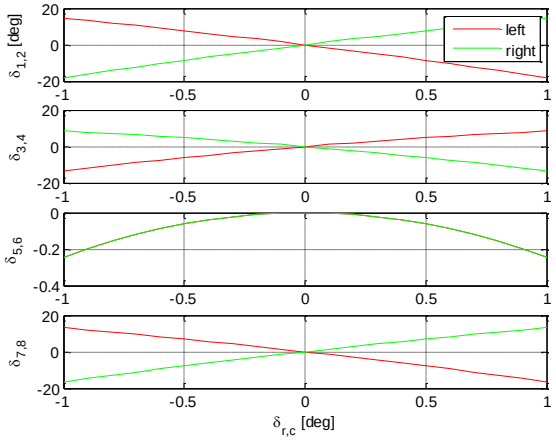

Fig. 6. Rudder mixing

Figure 6 presents the control surfaces deflections for a range of yaw control input. The yaw control mixing is relatively complex and would have been very difficult to design manually. A positive yaw control input (yaw to the right), results in the control surfaces on the left front wing deflecting upwards which is counter-intuitive, whereas the control surfaces on the left rear wing are deflected downwards, which was expected from an inspection of the aerodynamic data. The behaviour is most likely governed by the equality constraints that attempt to minimise the initial roll response to a yaw command. The control surfaces on the front wing are therefore deflected in the opposite direction than what was expected to yaw the aircraft. The figure also shows that control surfaces 5 and 6 were used very little in yawing the aircraft, once again as the optimiser mostly reserved these for pitch control.

The remaining elevator authority was determined by decreasing the airspeed from cruise to stall speed. The resulting control surface deflections are illustrated in Figure 7.

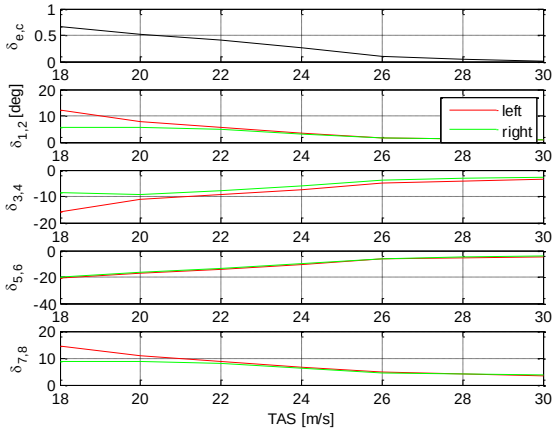

Fig. 7. Elevator control surface deflections at various airspeeds

The stall speed of the aircraft was at the nominal mass and standard sea-level conditions were 16 m/s. The figure above shows that a sufficient amount of elevator authority remains at the lowest trimmable airspeed

The aircraft's lateral response for a pure roll input is illustrated in Figure 8:

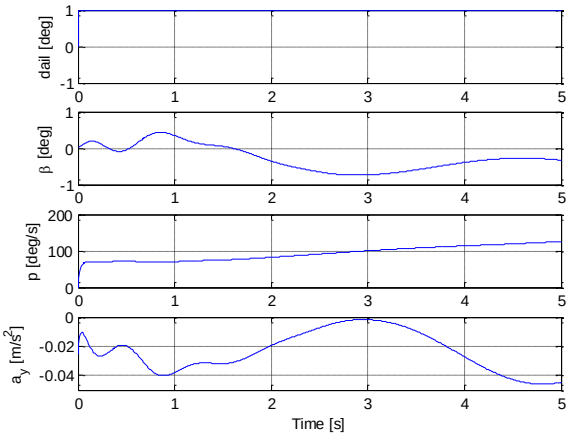

Fig. 8. Lateral response for a pure roll input

A steady roll rate (p) is reached within 0.15 seconds after the control input is given. Very little rudder control is needed to coordinate the aircraft for the small side slip and lateral acceleration (a_y) generated during a roll manoeuvre.

The aircraft's lateral response for a pure yaw input is illustrated in Figure 9:

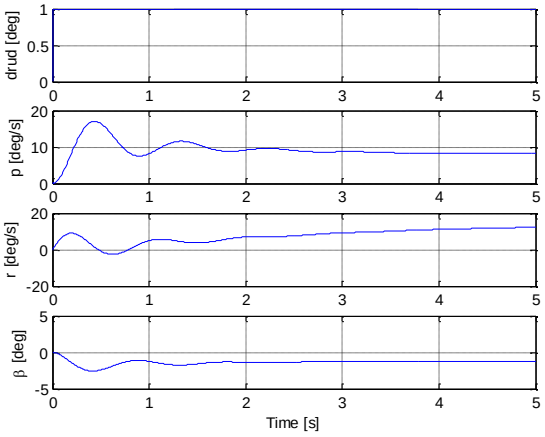

Fig. 9. Lateral response for a pure yaw input

The rudder generates a maximum yaw rate of approximately 9 deg /s. It can be seen that the rudder is not particularly effective, since a maximum rudder input is only able to generate an approximate steady-state sideslip angle of -1.3. However, the side slip generated for a roll input was very small, indicating that a sufficient amount of rudder would be available to coordinate the aircraft. There is no initial roll response to a yaw input. The longer term roll response to a yaw input is caused by the dihedral effect, which is a characteristic of the airframe.

5 Conclusion

A study was performed to evaluate various open-loop control allocation schemes for a UAV with a rhomboid wing configuration.

A sophisticated, non-linear 6 DOF flight dynamics model was assembled from wind tunnel data. The wind tunnel testing utilised a MDOE method, which present various challenges in order to develop a suitable flight dynamics model. The static derivatives were obtained in the form of coefficients of polynomial expressions and presented in the form of non-linear MDOE models. The MDOE models were manipulated by removing the asymmetric terms in order to model a symmetrical aircraft. The dynamic derivatives were obtained through AVL.

The design process required the use of constrained mathematical optimization in a two phase process. The first phase was used to determine the nominal trim terms, while the second phase was used to optimise the control response while taking handling qualities considerations into account.

All the constraints and handling quality specifications were satisfied at the optimum solution presented as an example in this paper. The work conducted to date will be further expanded to obtain scheduled mixing programs, utilising a similar process but for a series of flight conditions. Scheduling will typically be implemented as a function of air speed. Through the use of alternative combinations of constraints and objective, it will also be possible to implement unconventional or special control modes, such as high-lift devices or direct force control.

References

[1] Basson L. *Control Allocation As Part of a Fault-Tolerant Control Architecture for UAVs*. Stellenbosch University, 2011.

[2] Haghighat S, Liu HHT and Martins JRRA. *Mixed-Norm Multi-Objective Robust Controller Applied to a Very Flexible Aircraft*. University of Michigan, 2011.

[3] Joshi M, Patre P, NASA Langley Research Centre, and Tao, G. University of Virginia. *Adaptive Control of Systems with Actuator Failures Using an Adaptive Reference Model*, 2012.

[4] Drela M and Youngren H. 2004. *AVL*. [online] Available at: http://web.mit.edu/drela/Public/web/avl [Accessed 07 01 2014].

[5] DeLoach R. *Application of Modern Experiment Design to Wind Tunnel Testing at NASA Langley Research Centre*. AIAA, 98-0713, 1998.

[6] Giunta A, Wojtkiewicz SF Jr and Eldred MS. *Overview of Modern Design of Experiments Methods for Computational Simulations.* AIAA 2003-0649.

[7] Dias JF, Broughton BA and Suleman A. *Aircraft Wind Tunnel Characterisation Using Modern Design of Experiments.* AIAA, Boston, Massachusetts, 2013-1502.

[8] Skinner PJ. *Low-speed Wind Tunnel Test of the Roadrunner Joined Wing Configuration*. Council for Scientific and Industrial Research, Pretoria, South Africa, 2014.

[9] Landman D, Simpson J, Mariani R, Ortiz F and Brithcher C. Hybrid Design for Aircraft Wind-Tunnel Testing Using Response Surface Methodologies. *Journal of Aircraft*, Vol. 44, No. 4, pp 1214-1221, 2007.

[10] Arora JS. *Introduction to Optimum Design*. 3rd edition, Academic Press, 2012.

[11] Department of Defence. *Flying Qualities of Piloted Airplanes*, MIL-F-8785C, 5 November 1980.

[12] Phillips WF. *Mechanic of Flight*. 2nd Edition, John Wiley & Sons, Inc, 2010.

Acknowledgements

The author would like to place on record thanks to the Council for Scientific and Industrial Research, Aeronautic Systems Competency that has funded and supported this project.

Copyright Statement